Superacidity and spectral signatures of hydroxyl groups in zeolites

Georgi N Vayssilov, Hristiyan A Aleksandrov, Eddy Dib, Izabel Medeiros Costa, Nikolai Nesterenko, Svetlana Mintova

Microporous and Mesoporous Materials 343 (2022) 112144

Contents lists available at ScienceDirect

Microporous and Mesoporous Materials

journal homepage: www.elsevier.com/locate/micromeso

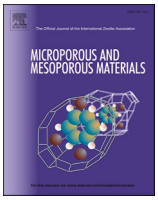

Superacidity and spectral signatures of hydroxyl groups in zeolites

Georgi N. Vayssilov [a,*], Hristiyan A. Aleksandrov [a,1], Eddy Dib [b,1], Izabel Medeiros Costa [c], Nikolai Nesterenko [c], Svetlana Mintova [b,**]

[a] Faculty of Chemistry and Pharmacy, University of Sofia, 1126, Sofia, Bulgaria
[b] Laboratoire Catalyse & Spectrochimie (LCS) Normandie Univ, ENSICAEN, UNICAEN, CNRS, 14000, Caen, France
[c] Total Energies Research and Technology, Feluy, B-7181, Seneffe, Belgium

ARTICLE INFO

Keywords:
Zeolites
Acidity
Hydroxyl groups
Silanols
Brønsted acid sites

ABSTRACT

The hydroxyls, Brønsted acid sites (BAS) and silanols, provide key contributions in the global acidity of zeolites and have significant impact on their properties and applications. In this work, we present the acidity of BAS and silanols in zeolites depending on their configurations in zeolite nanoparticles. The acidity was evaluated based on the deprotonation energy (DPE) calculated by the density functional method and compared to experimental spectra. The calculated DPE and available experimental data for acidity of small molecules in a gas phase allowed us to position the hydroxyl groups in zeolites into the general scale of gas phase acidity for the first time. The simulated deprotonation enthalpies for the bridging hydroxyls are in the range 1113–1187 kJ/mol while for silanols they vary in larger range 1186–1376 kJ/mol. Compared to gas phase acids, these values imply that the Brønsted acid sites fall in the range of superacids while silanols cover wide range from strong acids to superacids. The high gas phase acidy of the zeolite hydroxyls may be explained with the flexibility of the zeolite framework that efficiently accommodates the negative charge of deprotonated center via structural relaxation, electron density redistribution or formation of hydrogen bonds. Nanosized zeolite in proton form (HZSM-5) was used as a model system, and the proximities between bridging hydroxyls and ^{27}Al centers was estimated by ^{1}H{^{27}Al} REAPDOR MAS NMR technique. A linear correlation between the ^{1}H NMR chemical shifts and stretching O–H vibrational frequencies of the BAS was found similar to the silanol groups. However, no correlation between the deprotonation energy and the spectral characteristics of the corresponding hydroxyl (BAS and silanols) was observed. Thus, the acidity of the hydroxyls cannot be estimated based on the spectral characteristics, which accounts mainly for the formation and strength of hydrogen bonds.

1. Introduction

Zeolites are crystalline microporous aluminosilicate materials used as acid catalysts and sorbents in *inter alia* petrochemical industrial processes [1]. Their intrinsic acidity is due to the presence of aluminum in tetrahedral configuration within the siliceous framework giving rise to a negative charge, compensated by protons [2]. These acid sites – bridging hydroxyl groups, Al–OH–Si, acting as Brønsted acid sites (BAS), confer a high activity to zeolites [3]. Furthermore, another type of hydroxyl groups – silanols, Si–OH, exist in zeolites and their amount is sometimes far from negligible. The latter considered as structural defects are often neglected when considering the global acidity of zeolites despite the variety of configurations they present and their impact on final properties and applications [4].

Among the best characterization techniques used to probe hydroxyl groups in solids are ^{1}H solid-state nuclear magnetic resonance (NMR) and infrared (IR) spectroscopy [5]. The vibration frequency of OH groups in IR as well as their proton chemical shift in NMR vary with the strength of hydrogen bonds in which they are involved when present. Isolated silanols and bridging hydroxyl groups (not involved in a hydrogen bond), present stretching vibrational frequencies around 3745 cm^{-1} and 3615 cm^{-1} respectively, that decreases when hydrogen bonding occurs. The corresponding ^{1}H NMR chemical shifts are ~1.8 and ~4 ppm, however, these values increase when hydrogen bonds occur. Then, the quantification and identification of these sites was never a trivial task because of signal overlapping [6,7]. Several

* Corresponding author.
** Corresponding author.
E-mail addresses: gnv@chem.uni-sofia.bg (G.N. Vayssilov), svetlana.mintova@ensicaen.fr (S. Mintova).
[1] Equally contributed.

https://doi.org/10.1016/j.micromeso.2022.112144
Received 5 July 2022; Received in revised form 24 July 2022; Accepted 26 July 2022
Available online 8 August 2022

combinations of experimental and theoretical methods including IR, NMR and density functional theory (DFT) calculations were considered to resolve those issues. Advanced NMR techniques have been used to distinguish isolated and hydrogen bonded BAS in selected zeolites due to the paramount importance of those sites for catalysis [7–10]. Other NMR approaches were explored to localize aluminum or silanols with respect to structure directing agents in as synthesized zeolites [11,12].

Since zeolites are applied in most industrial processes as solid acid catalysts, their acidity is extensively studied using spectroscopic, sorption, thermal and catalytic approaches [6,13]. All those methods applied to zeolites, however, in addition to the intrinsic acidity of the measured hydroxyl groups, various additional effects e.g. confinement, adsorption and diffusion were considered [14–17]. A direct measure of the acidity of a hydroxyl group in a chemical compound is its deprotonation energy (DPE), namely the enthalpy of the reaction

$$XO\text{-}H \rightarrow XO^{-} + H^{+}$$

which can be measured experimentally for molecules in the gas phase [18]. Since for hydroxyl groups in solid, as zeolites, such direct measurement of the DPE cannot be performed, the corresponding values have been approached by computational methods. Following the pioneering calculations of Sauer [19] and van Santen [20], several groups reported computed DPE values for zeolites with different framework structures and aluminum content. The simulations evolved from isolated fragments of the zeolite framework to embedded models and periodic 3-dimensional models [10,21–25]. Typically, the calculated DPEs of BAS are around 1100–1250 kJ/mol but they vary depending on the computational method and models used.

In this study, the acidity of various silanol groups and BAS in nanosized HZSM-5 zeolite was evaluated based on the deprotonation energy calculated using DFT with hybrid functional PBE0 in order to understand their contribution to the global acidity of zeolites. While BAS act as strong acids, the silanols may behave as milder acid sites, which are beneficial for some catalytic or sorption processes requiring moderate acidity [26]. Using available experimental values for deprotonation energy of small molecules in the gas phase and the calculated DPE values, we estimated the real deprotonation enthalpy of the hydroxyl groups in nanosized HZSM-5 zeolite. The nanosized zeolite was synthesized and characterized using a combination of spectroscopic approaches (see Supplementary Information). Based on the experimental and theoretical results, a proper positioning of BAS and silanols in zeolites into the general scale of gas phase acidity is proposed.

2. Methods

2.1. Computational details

Quantum chemical calculations were based on Density functional theory approach with the hybrid gradient-corrected PBE0 exchange-correlation functional [27] using ORCA, ab initio, DFT and semi-empirical electronic structure package (vers. 4.1.2) [28,29]. The atomic basis sets for geometry optimization were def2-SVP basis set with utilization of def2/J auxiliary basis [30,31]. No restrictions on the atomic positions, interatomic distances or angles were applied during geometry optimization. For the calculations reported here, we used all-silica ZNP-99, ZNP-111 and ZNP-165 models described in our previous work [32]. The initial structures of the Al-containing zeolite nanoparticles models used here, AlZNP-99, AlZNP-111a, AlZNP-111b, AlZNP-111ab, were constructed from the corresponding all-silica models as one or two Si centers were replaced by Al to create bridging hydroxyl groups acting as Brønsted acid sites (Fig. 1). The aluminum center in AlZNP-99 and Ala in AlZNP-111a and in AlZNP-111ab models are bound via oxygen bridges to Si centers of the nanoparticle, while Alb at AlZNP-111b and AlZNP-111ab models is located at the surface of the nanoparticle and is bound to one terminal hydroxyl and to three Si centers via oxygens.

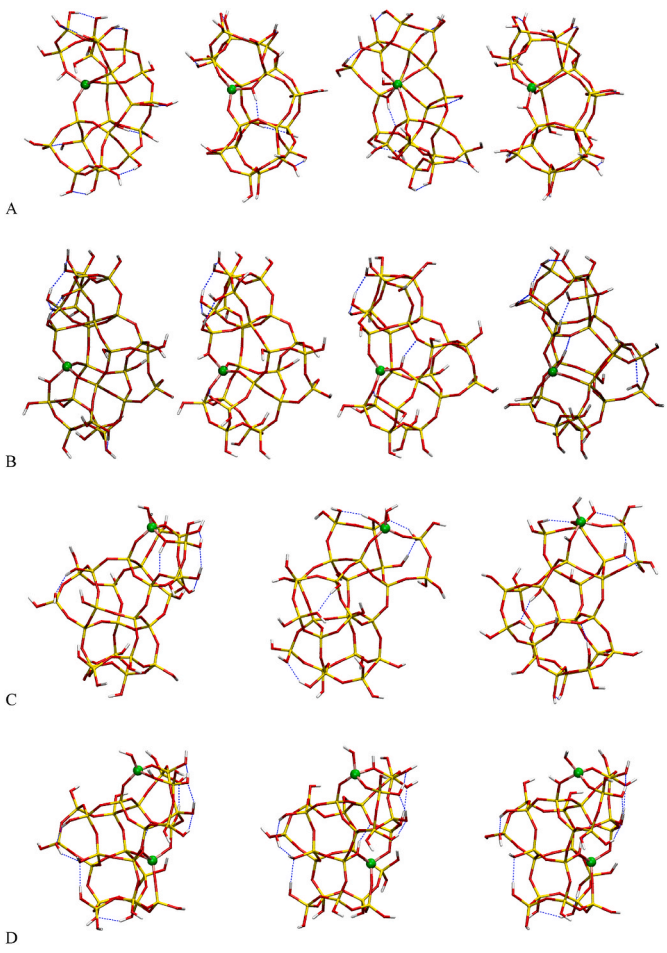

Fig. 1. Optimized structures of zeolite nanoparticles with MFI type framework containing 1 or 2 Al centers: (A) AlZNP-99, (B) AlZNP-111a, (C) AlZNP-111b, (D) AlZNP-111ab with different locations of the Brønsted centers (Al centers in green, linear hydrogen bonds in blue). (For interpretation of the references to color in this figure legend, the reader is referred to the Web version of this article.)

The frequency calculations for all models were preformed numerically and the calculated values for stretching vibrational frequencies of O–H groups were scaled in standard fashion with a scaling factor 0.948 to correct them for the anharmonicity and the shifts due to the computational method, as reported earlier [32].

The ^{1}H NMR chemical shifts were calculated with Gauge-Independent Atomic Orbitals (GIAOs) method [33], using auxiliary basis def2/JK, Grid4 FinalGrid5, and tighter SCF convergence criteria. The chemical shift values were obtained by subtraction from the calculated isotropic chemical shielding value for tetramethylsilane (TMS).

2.2. Synthesis and characterizations

The nanosized ZSM-5 zeolite was synthesized using a clear precursor suspension with the following chemical composition: 1 SiO_2: 0.25 TPAOH: 25H_2O: 0.0125 Al_2O_3: 0.05 Na_2O. For the preparation of the suspensions, the total amounts of double distilled water and organic structure directing agent (tetra n-propylammonium hydroxide (TPAOH), 20 wt % in water solution, Alfa Aesar) were mixed for about 15 min using magnetic stirring. Then, the silicon source (tetraethyl orthosilicate (TEOS) 98%, Aldrich) was added dropwise to the suspension and subjected to magnetic stirring for 1 h. Finally the aluminum source (aluminum nitrate ($Al(NO_3)_3.9H_2O$, 97%, Prolabo) was added to

the suspension followed by aging on an orbital shaker for 18 h at room temperature. Then, the hydrothermal treatment was carried out in Teflon-lined stainless-steel autoclaves at 180 °C for 72 h under autogenous pressure. The solids were purified with double-distilled water and high-speed centrifugation, until the pH of the supernatant was below 8. The samples were dried at 90 °C and calcined at 550 °C/5h in air.

^{29}Si and ^{27}Al magic-angle spinning (MAS) NMR experiments are performed at 99.3 and 130.3 MHz, respectively on a 500 MHz (11.4 T) Bruker Avance III-HD spectrometer using a 4 mm probe head, the sample is rotated at 14 kHz spinning rate. (Figs. S1A and B in Supplementary data). The chemical shifts for silicon and aluminum are referenced to tetramethyl silane (TMS) and $AlCl_3$, respectively. Radio frequency (rf) field strength of 36 and 50 kHz and recycle delays of 20 and 1 s, respectively were used.

^{1}H simple pulse, ^{1}H{^{27}Al} TRAPDOR and ^{1}H{^{27}Al} REAPDOR (MAS) NMR experiments were performed using the 4 mm probe head. ^{1}H chemical shifts are referenced to TMS. A radio frequency (rf) field strength of 50 kHz is used for ^{1}H ($\pi/2$ pulse of 5 μs). For REAPDOR measurements, the adiabatic pulse length used for the ^{27}Al channel is equal to 1/9 of the rotor period (8.88 μs), and the spinning rate is set to 12.5 kHz. The recycle delay is set to 10 s. For ^{1}H NMR measurements all the samples were pre-treated under vacuum at 350 °C overnight prior to filling into the rotor in an Argon saturated glove box. Spectral deconvolution and numerical simulations were performed using Dmfit [34] and SIMPSON [35].

The crystallinity of the sample was investigated by powder X-ray diffraction (Fig. S1C in Supplementary data) by a PANalytical XPert Pro diffractometer using Cu Kα radiation ($\lambda = 1.5418$ Å, 45 kV, 40 mA). The FTIR spectra are acquired using a Nicolet Magna 550-FT-IR spectrometer (4 cm^{-1} optical resolution). The IR spectrum corresponds to *in situ* activated sample at 350 °C under vacuum.

3. Results and discussions

3.1. Spectral features of the bridging hydroxyls

The nanosized ZSM-5 (Si/Al = 40) present an average size of 100 nm and show high crystallinity with mainly tetrahedral aluminum in the framework (Fig. S1 in Supplementary data). The corresponding ^{1}H NMR and IR spectra are depicted in Fig. 2A and C, respectively. The spectra contain the characteristic bands for silanols (~3740–3700 cm^{-1}, 1.5–2.4 ppm) and BAS (3630 cm^{-1}, 3.7 ppm). This is confirmed by NMR using a Transfer of Populations in Double Resonance (TRAPDOR) indicating a loss in the intensity of the signal at 3.7 ppm after irradiation of Al during the echo evolution time while the peaks corresponding to silanols keep the same intensity except for the band at 2.4 ppm suggesting the presence of Al in their vicinity (Fig. 2B). The dipolar modulation, giving rise to the intensity loss (difference between S_0 and S) is introduced during the evolution time thanks to a dephasing pulse applied on ^{27}Al in the pulse sequence. The same methodology was used for the REAPDOR experiment, known to be more robust and less sensitive to diverse Al environments that may be present within the framework. The distance between proton and aluminum was determined based on this experiment (3.7 ppm) and the corresponding $\Delta S/S_0$ curve simulated using SIMPSON code [35] is shown in Fig. 2D; the remaining three peaks kept the same intensity during the evolution time. The strong slope before 1000 μs corresponds to the highest dipolar modulation, mainly due to a coupling of ~2 kHz corresponding to a distance ^{1}H—^{27}Al of ~2.5 Å. The weak slope observed between 2000 and 5000 μs indicates the presence of other Al neighbors located at longer distances estimated at ~5 Å in line with the previous study reported by Koller and coworkers [10]. This explains the slight difference between experimental and simulated curves for high evolution times. The spins considered for the simulation were a pair of ^{1}H and ^{27}Al with a dipolar coupling of 2 kHz that corresponds to the first neighbors. However, other hydrogen bonded BAS and SiOH appear in different zeolites as stated above and the correlation between their spectral features and acidity is of paramount importance.

Quantum chemical calculations, reported here, were based on Density functional theory approach with the hybrid gradient-corrected PBE0 exchange-correlation functional. We used all-silica ZNP-99, ZNP-111 and ZNP-165 models as described in our previous work [32]. The structures of the Al-containing zeolite nanoparticles (AlZNP-99, AlZNP-111a, AlZNP-111b, AlZNP-111ab) were constructed from the corresponding all-silica models as one or two Si centers were replaced by Al to create bridging hydroxyl groups acting as Brønsted acid sites. The aluminum center in AlZNP-99 and Ala in AlZNP-111a and in AlZNP-111ab models are bound via oxygen bridges to Si centers of the nanoparticle, while Alb at AlZNP-111b and AlZNP-111ab models is located at the surface of the nanoparticle and is bound to one terminal hydroxyl, forming Al–OH moiety, and to three Si centers via oxygens (Fig. 1).

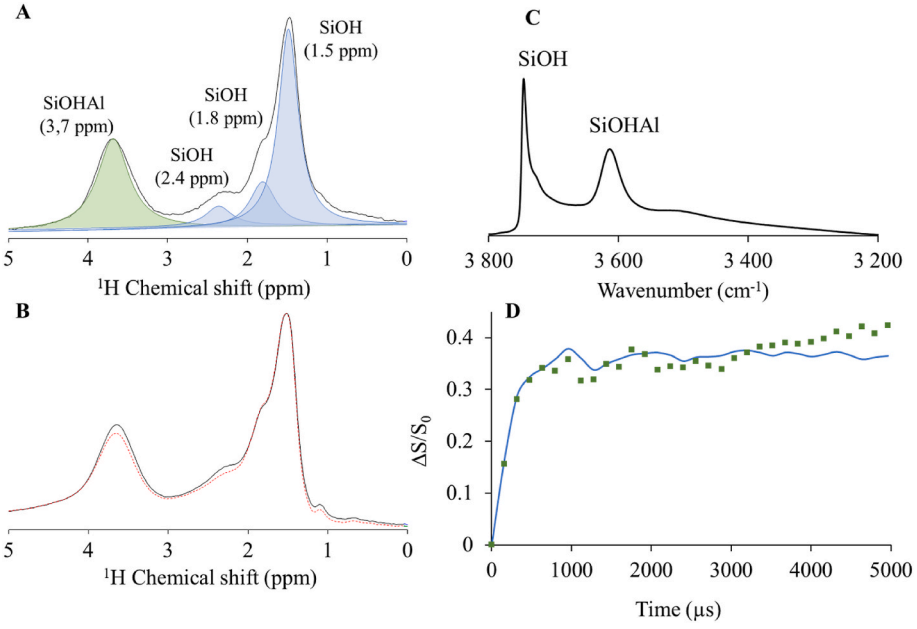

Fig. 2. A. Single pulse ^{1}H NMR spectrum of nanosized HZSM-5 zeolite: the spectrum is deconvoluted and the peaks are assigned to SiOH (blue) and BAS (green). B. TRAPDOR effect on the ^{1}H NMR spectrum: the solid line corresponds to two rotor periods echo without irradiation of Al and the red dashed line corresponds to the same echo with Al irradiation. C. FTIR spectrum of activated nanosized HZSM-5 zeolite. D. REAPDOR curve (dots) and the corresponding numerical simulation (solid line) for the peak at 3.7 ppm in the ^{1}H NMR spectra. The simulation corresponds to a pair of ^{27}Al and ^{1}H spins with a dipolar coupling of 2 kHz. (For interpretation of the references to color in this figure legend, the reader is referred to the Web version of this article.)

Vibrational frequencies and ^{1}H NMR chemical shifts of all bridging hydroxyls (Si–OH–Al) and various silanols (Si–OH) were calculated. For the BAS, three types of hydroxyls were identified considering their spectral features and involvement in hydrogen bonds (see Fig. 3A and B). The first type corresponds to isolated BAS with O–H vibrational frequency between 3620 and 3646 cm^{-1} and ^{1}H NMR shift between 3.36 and 3.70 ppm. Those hydroxyls do not participate in regular hydrogen bonds and neighboring framework oxygens are more than 250 pm far away from the acidic proton. They correspond to the classical BAS with experimentally measured IR frequency around 3630 cm^{-1} and $\delta(^1H)$ around 3.7 ppm, as reported above (Fig. 2A, C). The distance between the Al center and the proton from the corresponding bridging hydroxyl group is in the range 233–253 pm that is in an agreement with the REAPDOR-NMR results shown in Fig. 2D. The second type of BAS corresponds to hydroxyls with vibrational frequency of 3400–3600 cm^{-1} and $\delta(^1H)$ varying between 3.80 and 5.70 ppm. These bridging hydroxyls do not participate in a regular hydrogen bond, for which the arrangement O–H···O is close to linear. However, their protons are affected by the oxygens located aside at H···O distances between 200 and 240 pm, which may be considered as irregular (side) hydrogen bonds with O–H···O angles up to 120°. The third type of BAS corresponds to hydroxyls with regular linear hydrogen bonds to oxygen centers in the opposite side of the zeolite ring, which in our models has an O–H frequency between 2950 and 3230 cm^{-1} and $\delta(^1H)$ varying from 7.30 to 10.04 ppm.

Interestingly, the plots of the O–H stretching frequency (Fig. 3A) and ^{1}H NMR chemical shift (Fig. 3B) of the modeled bridging hydroxyls versus the distance between the BAS proton and the closest oxygen center corresponding to two types of hydroxyls are well aligned in a parabola. This suggests that the regular hydrogen bonds and the irregular hydrogen bonds to side oxygens affect the spectral signatures of the corresponding hydroxyl in the same way.

The trends for the calculated ^{1}H NMR chemical shift of BAS versus the hydrogen bonding distance has the same shape as that for silanols, reported earlier [32] (see Fig. 3C). The only difference is that for the same hydrogen bonding distance, the ^{1}H NMR chemical shifts of the bridging hydroxyls are about 1.5 ppm higher than the silanols protons, while for protons participating in very strong hydrogen bonds (H-bond below 170 pm) this difference almost vanishes. This implies that the linear correlation between hydrogen bond length and $\delta(^1H)$ suggested by Yesinowski et al. for hydroxyl groups in solids [36], has to be reconsidered. Instead, one may derive separate linear equations for the BAS acid sites with strong (linear) hydrogen bonds and those participating in side (medium) hydrogen bonds at $\delta(^1H)$ = 28.855–0.118 (H-bond, in pm) and $\delta(^1H)$ = 11.824–0.0326 (H-bond), respectively. The coefficients in the two equations are similar to those recently reported for silanol groups participating as proton donors in strong and medium hydrogen bonds, i.e. $\delta(^1H)$ = 25.39–0.108 (H-bond, in pm) and $\delta(^1H)$ = 12.464–0.0419 (H-bond), respectively (see Supplementary information of Ref. 32). Analogous trend is observed for the calculated vibrational frequencies of the hydroxyl as a function of the hydrogen bonding distance (not shown here) – the ν(O–H) for the BAS participating in hydrogen bond is about 100 cm^{-1} lower than the frequency of the silanol, participating in hydrogen bond with the same H-bonding distance.

In Fig. 3D one can see that the linear correlation between vibrational frequency and the chemical shift of the proton of specific hydroxyl, observed earlier for silanols [32], ν(O–H) = 3868.3 – (84.989) $\delta(^1H)$ NMR, was also found for the bridging hydroxyl, with somewhat different coefficients: ν(O–H) = 4016 – (106.84) $\delta(^1H)$ NMR (with RMSD = 0.99). As shown, the data points for bridging hydroxyls fall essentially in the same region as that for the silanols: $\delta(^1H)$ higher than 3.0 ppm and ν(O–H) lower than 3650 cm^{-1}. Thus, based on the vibrational frequency or $\delta(^1H)$ NMR in those regions one cannot unambiguously identify if the specific hydroxyl is a silanol or a BAS. Experimentally both types of hydroxyls with sharp peaks at 3745 and 3615 cm^{-1} can be distinguished in the IR spectra if they do not participate in hydrogen bonds. However, when the hydroxyls participate in hydrogen bonds, the bands for both types of hydroxyls are wider and cannot be discriminated easily. In Fig. 3D one can also see the points corresponding to the spectral characteristics of the terminal Al–OH group in the AlZNP-111b model with different locations of the charge compensating protons at the bridging oxygen centers. Since Al–OH group does not participate in hydrogen bonds, both the IR frequencies and ^{1}H chemical shifts vary in narrow ranges, from 3774 to 3799 cm^{-1} and from 0.00 to 0.43 ppm, clearly different from silanols and bridging hydroxyls.

3.2. Acidity of bridging hydroxyls and silanols

As described above, the acidity of BAS and silanols is evaluated by

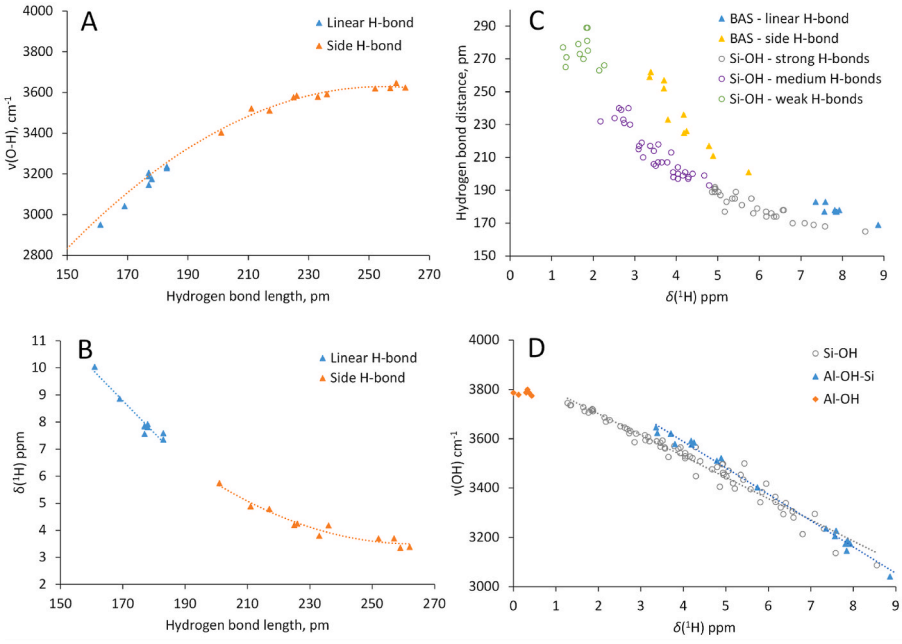

Fig. 3. Plots of the correlations between calculated spectral features of the modeled hydroxyls and their participation in hydrogen bonds: (A) O–H stretching frequency vs. hydrogen bonding distance for BAS; (B) ^{1}H NMR chemical shift vs. hydrogen bonding distance for BAS; (C) hydrogen-bonded distance in BAS or silanols vs. ^{1}H NMR chemical shift; (D) O–H stretching frequency and ^{1}H NMR chemical shift of BAS or silanol. Symbols corresponding to different types of hydroxyl groups are shown as insets.

calculating the DPE of these groups in the modeled zeolite nanoparticles. The obtained deprotonation energy of the bridging hydroxyl sites in the AlZNP models are varying between 1164 and 1242 kJ/mol depending on both the positions of Al and the acidic proton considered in the model. Recently, Koller et al. reported deprotonation energies of a series of bridging OH groups in SSZ-42 zeolite between the 1157–1187 kJ/mol using PBE-D3/def2-TZVP method [10]. They suggested that the DPE correlates with ^{1}H NMR chemical shift of their protons with some deviation; the higher ^{1}H chemical shift corresponds to higher deprotonation energy. However, our results show that scattering dominates over any correlation of the calculated deprotonation energy with the simulated ^{1}H NMR chemical shifts of hydroxyl groups (see green triangles in Fig. 4A). This is valid for both silanols and bridging hydroxyls. No correlation was observed also between the deprotonation energy and O–H stretching frequency of the hydroxyl group (Fig. 4B), as also reported elswere [25].

The lowest deprotonation energy of 1164 kJ/mol, corresponding to the most acidic BAS, is obtained for the AlZNP-111a structure, in which the deprotonated hydroxyl initially participates in a strong hydrogen bond to a zeolite oxygen center within a five-membered ring. However, the other bridging hydroxyls participating in strong hydrogen bonds feature diverse values of the deprotonation energies between 1172 and 1242 kJ/mol (triangles with $\delta(^1H)$ between 7 and 10 ppm in Fig. 4A and O–H frequencies between 3250 and 2940 cm^{-1} in Fig. 4B). The bridging hydroxyls, which are not involved in hydrogen bonds have deprotonation energy values in the same range, 1171–1225 kJ/mol (triangles with $\delta(^1H)$ around 4 ppm in Fig. 4A and around 3600 cm^{-1} in Fig. 4B). The BAS with the strongest hydrogen bonds have deprotonation energies of 1191 and 1242 kJ/mol (triangle at $\delta(^1H)$ of 8.89 and 10.04 ppm). **These results show clearly that the participation of a bridging hydroxyl in hydrogen bonds cannot be directly related to the acidity of that group as estimated by the deprotonation energy value.**

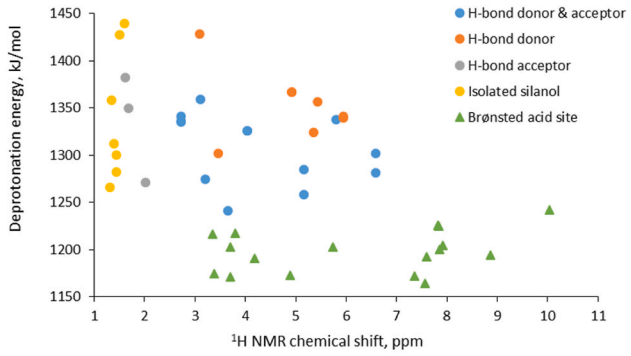

A

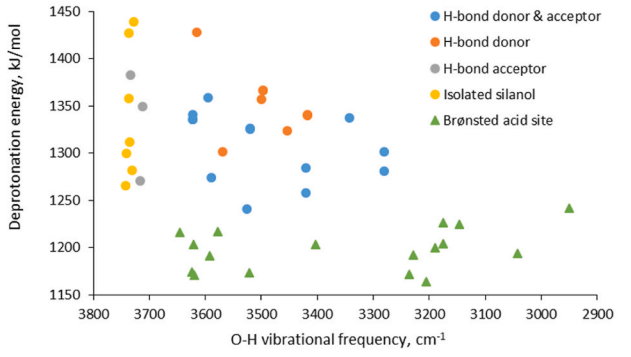

B

Fig. 4. Calculated deprotonation energy of a silanol and bridging hydroxyl groups versus ^{1}H NMR chemical shift (A) and OH vibrational frequency (B) of that hydroxyl group. Symbols, corresponding to different types of hydroxyl groups are shown in the legend inside the panel.

One may also compare the average values of the DPE of the bridging hydroxyls around each of the modeled Al positions, which may be related to the acidity potential of that Al site, i.e. if the bridging hydroxyls at this center may produce more or less acidic BAS. In our AlZNP models we have four Al sites (AlZNP-99, AlZNP-111a, AlZNP-111b, and Alb at AlZNP-111ab), which have average DPE values of 1225, 1176, 1210, and 1189 kJ/mol, respectively. The values for Alb at AlZNP-111ab were calculated with one position of the BAS at Ala in the model and different positions of the bridging hydroxyl around Alb center. Thus, both the lowest and the highest average DPE values correspond to the inside Al centers with four Si centers as next nearest neighbors.

The deprotonation energy values calculated for different types of silanols are spread in a larger interval 1241–1439 kJ/mol (about 200 kJ/mol), than for the values of the bridging hydroxyls 1164–1242 kJ/mol (about 80 kJ/mol). Some of the silanols exhibit low deprotonation energies values that overlap with the less acidic bridging hydroxyls (BAS) as shown in Fig. 4. Note that during the optimization of the geometry of the deprotonated nanoparticle there was reorientation of the silanols around the negatively charged oxygen, and in some cases a proton shift from a neighboring silanol to that oxygen center occurs. Thus, the deprotonated silanol in the final structure may differ from the initially deprotonated one. Interestingly, the participation of silanols in hydrogen bonds as proton donors, proton acceptors or both, is not related to the DPE calculated (see the circles with different colors in Fig. 4). Similarly, to the BAS, no correlation was observed between the deprotonation energy and the spectral characteristics of silanols (^{1}H NMR chemical shift and O–H stretching frequency of hydroxyl groups) either.

4. Discussion

The lack of correlations between deprotonation energies and spectral features of silanols can be explained by the dominant influence of the final state, namely more or less efficient stabilization of the negatively charged oxygen center remains after deprotonation. The stabilization may be achieved by local structural rearrangement around the negatively charged oxygen or by the formation of hydrogen bonds to it from neighboring hydroxyls, if available. When the deprotonated silanols form new hydrogen bonds with neighboring silanols, the negative charge of the oxygen is partially compensated by the positive charge of the proton, which leads to stabilization of deprotonated structure. Similar stabilization effect has been shown to increase the acidity of Brønsted acid sites in mixed sodium and protonic forms of zeolites due to stabilization of the deprotonated state by compensating the negative charge of the oxygen by neighboring sodium ion [37]. In order to highlight the contribution of the final state on the deprotonation energy of silanols via formation of hydrogen bonds, we counted the number of hydrogen bonds that compensate the negatively charged oxygen center of the deprotonated silanol (Fig. 5A). The highest DPE is calculated for deprotonated silanols that are not compensated by hydrogen bonds from neighboring silanols (around 1430 kJ/mol). By increasing the number of compensating hydrogen bonds to one, two and three, the calculated deprotonation energy decreases to 1326–1383 kJ/mol, 1260–1350 kJ/mol, and 1241–1280 kJ/mol, respectively. Since the strength of the compensating hydrogen bonds is different, the values for the deprotonated silanols, compensated by the same number of hydrogen bonds vary substantially.

The analysis of the factors affecting the deprotonation energies of the bridging hydroxyl should take into account that the final deprotonated state of the hydroxyl around a certain Al center is the same (see the triangles with different colors in Fig. 5B). Thus, for these hydroxyls, the initial state of the structure should have dominant contribution to the deprotonation energy, which can be decomposed into vertical DPE (the energy of the structure just after removal of the proton) and relaxation energy of the deprotonated structure. As shown in Fig. 5B, the points for the total DPE are spread even for hydroxyls, located around the same Al

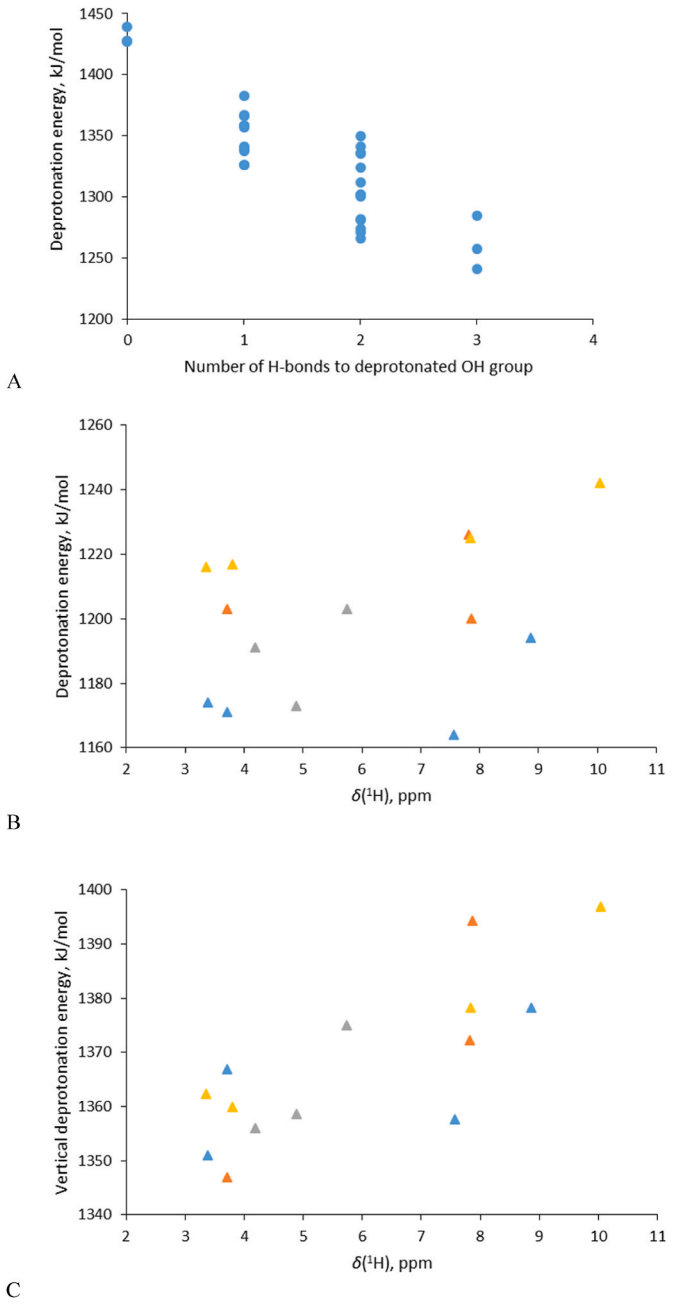

Fig. 5. Calculated DPE of a silanol versus the number of hydrogen bonds that compensate the negatively charged oxygen center of the deprotonated silanol (A) and calculated DPE (B) and vertical DPE (C) of bridging hydroxyl groups versus ^{1}H NMR chemical shift of that hydroxyl group in different AlZNP-99 (yellow triangles), AlZNP-111a (blue triangles), AlZNP-111ab (grey triangles) and AlZNP-111b (orange triangles) models. (For interpretation of the references to color in this figure legend, the reader is referred to the Web version of this article.)

center. In order to focus on the initial state influence on the DPE, we calculated vertical deprotonation energy values and found a rough trend, i.e. the lower ^{1}H NMR chemical shift of the proton corresponds to lower vertical DPE value (Fig. 5C). This trend is similar to that reported by Koller et al. for the total DPE values of SSZ-42 zeolite [10]. Note, however, that even for the vertical DPE the observed trend is still far from a good linear correlation (RMSD = 0.63). The reason for this is that both the ^{1}H chemical shift and the O–H vibrational frequency account only for the participation of the hydroxyl proton in hydrogen bond but are not related to other features of the initial state. For example, the formation of a hydrogen bond within a five-membered zeolite ring stabilizes the structure, e.g. makes the proton more difficult to be removed, however, to form a hydrogen bond, the $[AlO_4]^-$ tetrahedron and its surrounding are distorted, which contributes to destabilization of the structure. The experimentally measured spectral features, ν(O–H) and $\delta(^1H)$, account only for the first effect since it is connected with the strength of the hydrogen bond, but not for the second one. Thus, one may not expect strict correlations between the spectral features of hydroxyl groups with their deprotonation energies, and with their acidity respectively.

Fig. 6 schematically shows the ranges of calculated DPE values for the specific chemical shifts in the ^{1}H NMR spectrum measured for the nanosized HZSM-5 zeolite, as discussed above. From the experimental spectra one can derive the relative amount of the species with the corresponding chemical shift and their calculated deprotonation energy range.

As discussed in the introduction section, the DPE values for both BAS and silanol hydroxyl groups in zeolites cannot be measured directly and instead are evaluated by computational modeling. However, different computational approaches (method, model, system size) result in different values for analogous types of BAS. Similar problem appears in the calculation of vibrational frequencies, for which the calculated values for the studied system are corrected using experimental and calculated values for well-known simpler models as reference. Thus, employing the same computational approach for zeolite nanoparticles and a reference system, may allow after correction to estimate the real (experimental) values. The calculated values for deprotonation energies (DPE) and deprotonation enthalpy (DPΔH) of series of gas phase species containing hydroxyl group and their experimental DPΔH values are reported in Table S1; a part of the species includes Al–OH or Si–OH groups. For example, the calculated deprotonation energy and enthalpy for trimethylsilanol, $(CH_3)_3SiOH$ are 1589 kJ/mol and 1553 kJ/mol, respectively. The experimental deprotonation enthalpy values are somewhat lower, i.e. 1518 ± 19 kJ/mol and 1502 ± 17 kJ/mol as reported by Angelini et al. [38] and Damrauer et al. [39], respectively. For all gas phase species, the calculated DPΔH values overestimate the experimental ones (without taking into account the reported experimental accuracy margins) by 6–56 kJ/mol with an average overestimation of 34 kJ/mol. In the Table, the ratio between the

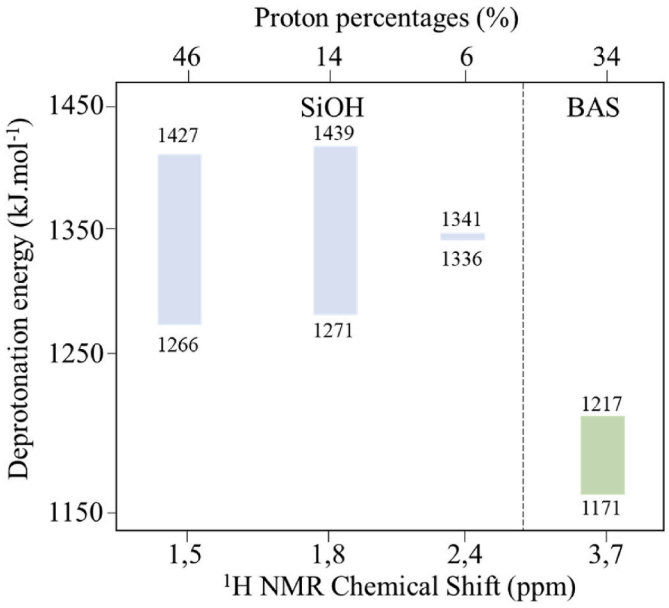

Fig. 6. Calculated DPE ranges corresponding to the main chemical shifts in the ^{1}H NMR spectrum experimentally observed (Fig. 2A) and the percentage of the corresponding species.

experimental DPΔH and calculated DPE values for each species (an average of 0.956) is provided. If we take into account only the species containing silicon or aluminum, the average scaling coefficient is essentially the same. Thus, we used the value 0.956 to scale the calculated DPE in order to estimate the real deprotonation enthalpy values of the hydroxyl groups in zeolites. As shown in Table S1 in Supplementary data, the simulated DPΔH values from the calculated DPE values of the reference molecules multiplied by the scaling factor fall into the accuracy range for all but one gas phase species. This observation allowed us to use the same way to simulate the real DPΔH values for the hydroxyl groups in zeolites. For BAS, the estimated real deprotonation enthalpy based on the minimal and maximal calculated DPE of 1164 and 1242 kJ/mol is between 1113 and 1187 kJ/mol. For silanols the range of the estimated real deprotonation enthalpy is much larger, from 1186 to 1376 kJ/mol.

The estimated DPΔH values allow us to align the BAS and silanol hydroxyl groups in zeolite nanoparticles in the general scale of gas phase acidity. For this, we used both experimental DPΔH and calculated DPE values for several sulfur, phosphorous and carbon containing molecules (Fig. 7). This result suggests that the Brønsted acid sites in the zeolite fall in the range of superacids with gas phase acidity higher than fluorosulfuric and perchloric acids, and is similar to hexafluorophosphoric acid. The silanols in zeolite cover a wide range from strong acids to superacids overlapping with the acidity of nitric, phosphoric and sulfuric acids. The higher gas phase acidy of the zeolite hydroxyls, both bridging and silanol, compared to the gas phase species, may be explained with the flexibility (mechanical or electronic) of the zeolite framework that allow efficient redistribution of the negative charge of deprotonated center via structural relaxation, electron density redistribution or stabilization by hydrogen bonds from neighboring hydroxyls.

5. Conclusions

The results, reported here, have shown that ^{1}H NMR chemical shifts and stretching O–H vibrational frequencies of bridging hydroxyls in ZSM-5 zeolite follow the same linear correlation observed earlier for the silanol groups. Moreover, the calculated values of those spectral parameters of the bridging hydroxyls and silanols fall essentially in the same plot for ν(O–H) below 3640 cm^{-1} and δ(^{1}H) above 3.4 ppm. As expected, the decrease of the O–H frequency and increase of the ^{1}H chemical shift depends on the formation of hydrogen bond and correlates with the corresponding hydrogen bonding distance. Interestingly, this correlation involves not only the regular close to linear hydrogen bonds, but also irregular side hydrogen bonds with O–H···O angles up to 120°. Thus, the traditional assumption that hydrogen bonds should be close to linear, is not valid, at least for the studied systems.

The acidity of the bridging hydroxyls, estimated by their deprotonation energy, is in the range 1164–1242 kJ/mol, while the DPE values for silanols vary in larger range, 1241–1439 kJ/mol. The calculated acidity values suggest that some of the silanol groups have sufficient acidity, which is essential for the application of zeolites as acidic catalysts milder than BAS. These acid sites are highly required for a series of catalytic processes in which strong acid sites, as BAS, are undesirable.

No correlation was found between the deprotonation energy and the spectral characteristics of the corresponding hydroxyl neither for bridging hydroxyls nor for silanols. The reasons for this discrepancy, were different for the two types of hydroxyl groups. For silanols, the DPE value is substantially influenced by the stabilization of the deprotonated state, which can be accomplished by the formation of hydrogen bonds from near hydroxyl groups. This can explain why the spectral features, which are characteristic for the initial intact hydroxyl group, do not correlate with the DPE values. On the other hand, the deprotonation energy of BAS depends on the stability of the initial intact state since the final deprotonated state at a specific Al position is the same for all positions of the bridging hydroxyl groups around it. The lack of correlation with the spectral features of the hydroxyl in this case is due to the fact that these features reflect basically the strength of the hydrogen bonds only without considering the structural distortions occurring due to the formation of such bonds.

Using as references experimental and calculated values for well-known gas phase species we derived a scaling coefficient (for the specific method) allowing from the calculated DPE for hydroxyl groups in zeolites to estimate their experimental deprotonation enthalpies. The gas phase deprotonation enthalpy, obtained with this approach, for BAS is 1113–1187 kJ/mol, while for silanols it is 1186–1376 kJ/mol. Those values suggest that Brønsted acid sites in zeolites can be categorized as superacids in the gas phase while the silanol groups are placed between strong acids and superacids.

CRediT authorship contribution statement

Georgi N. Vayssilov: Validation, Methodology, Conceptualization, Writing - original draft. **Hristiyan A. Aleksandrov:** Methodology, Formal analysis, Conceptualization, Writing - review & editing. **Eddy Dib:** Methodology, Formal analysis, Conceptualization, Writing - original draft. **Izabel Medeiros Costa:** Supervision, Writing - review & editing. **Nikolai Nesterenko:** Funding acquisition, Writing - review & editing. **Svetlana Mintova:** Supervision, Funding acquisition, Conceptualization, Writing - review & editing.

Declaration of competing interest

The authors declare that they have no known competing financial

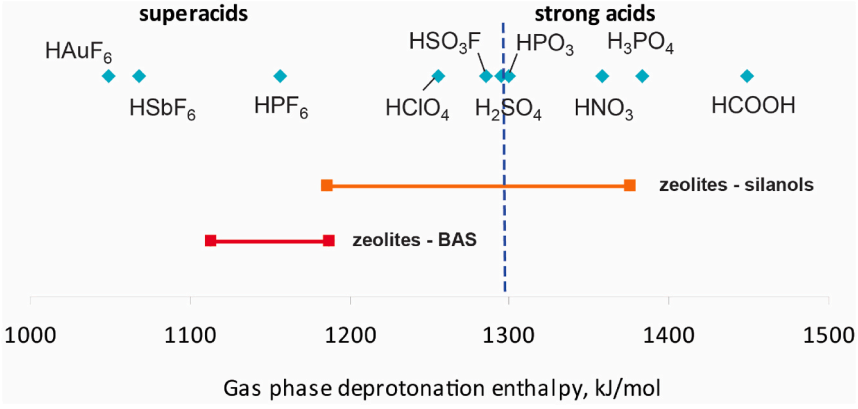

Fig. 7. Gas phase acidity scale of strong acids and superacids, including Brønsted acid sites and silanol groups in zeolite based on their simulated gas phase deprotonation enthalpies.

interests or personal relationships that could have appeared to influence the work reported in this paper.

Georgi N. Vayssilov reports financial support and travel were provided by Bulgarian Ministry of Education and Science. Hristiyan Aleksandrov reports financial support was provided by Bulgarian National Science Fund. Svetlana Mintova reports financial support was provided by Normandy Region. Svetlana Mintova reports financial support was provided by TotalEnergies SE.

Data availability

Data will be made available on request.

Acknowledgments

GNV acknowledges the support of the project EXTREME, funded by the Bulgarian Ministry of Education and Science (D01-76/March 30, 2021). HAA acknowledges the support by Bulgarian National Science Fund (project КП-06-H59/5). We acknowledge the support of the Label of Excellence for the Center for zeolites and nanoporous materials by the Region of Normandy (CLEAR) and Industrial Chair ANR-TOTAL "Nanoclean energy".

Appendix A. Supplementary data

Supplementary data to this article can be found online at https://doi.org/10.1016/j.micromeso.2022.112144.

References

[1] M. Guisnet, J.-P. Gilson, Zeolites for Cleaner Technologies. Catalytic Science Series, vol. 3, Imperial College Press, London, 2002, ISBN 1-86094-329-2.
[2] C.S. Csundy, P.A. Cox, The hydrothermal synthesis of zeolites: history and development from the earliest days to the present time, Chem. Rev. 103 (3) (2003) 663–702.
[3] E.G. Derouane, J.C. Védrine, R. Ramos Pinto, P.M. Borges, L. Costa, M. Lemos, F. Lemos, F. Ramoa Ribeiro, The acidity of zeolites: concepts, measurements and relation to catalysis: a review on experimental and theoretical methods for the study of zeolite acidity, Catal. Rev. Sci. Eng. 55 (4) (2013) 454–515.
[4] I.C. Medeiros-Costa, E. Dib, N. Nesterenko, J.-P. Dath, J.-P. Gilson, S. Mintova, Silanol defect engineering and healing in zeolites: opportunities to fine-tune their properties and performances, Chem. Soc. Rev. 50 (2021) 11156–11179.
[5] T. Steiner, The hydrogen bond in the solid state, Angew. Chem. Int. Ed. 41 (2002) 48–76.
[6] K. Hadjiivanov, Identification and characterization of surface hydroxyl groups by infrared spectroscopy, in: Fr C. Jentoft (Ed.), Advances in Catalysis, vol. 57, Academic Press, 2014, 99-318.
[7] A. Palcic, S. Moldovan, H. El Siblani, A. Vicente, V. Valtchev, Defect sites in zeolites: origin and healing, Adv. Sci. (2021), 2104414.
[8] C. Schroeder, V. Siozios, C. Mück-Lichtenfeld, M. Hunger, M. Ryan Hansen, H. Koller, Hydrogen bond formation of brønsted acid sites in zeolites, Chem. Mater. 32 (4) (2020) 1564–1574.
[9] L. Treps, C. Demaret, D. Wisser, B. Harbuzaru, A. Méthivier, E. Guillon, D. V. Benedis, A. Gomez, T. de Bruin, M. Rivallan, L. Catita, A. Lesage, C. Chizallet, Spectroscopic expression of the external surface sites of H-ZSM-5, J. Phys. Chem. C 125 (3) (2021) 2163–2181.
[10] C. Schroeder, S.I. Zones, M. Ryan Hansen, H. Koller, Hydrogen bonds dominate brønsted acid sites in zeolite SSZ-42: a classification of their diversity, Angew. Chem. Int. Ed. 61 (2022), e202109313.
[11] E. Dib, T. Mineva, E. Veron, V. Sarou-Kanian, F. Fayon, B. Alonso, ZSM-5 zeolite: complete Al bond connectivity and implications on structure formation from solid-state NMR and Quantum chemistry calculations, J. Phys. Chem. Lett. 9 (1) (2018) 19–24.
[12] E. Dib, J. Grand, S. Mintova, C. Fernandez, Structure-directing agent governs the location of silanol defects in zeolites, Chem. Mater. 27 (22) (2015) 7577–7579.
[13] W.E. Farneth, R.J. Gorte, Methods for characterizing zeolite acidity, Chem. Rev. 95 (3) (1995) 615–635.
[14] M. Boronat, A. Corma, What is measured when measuring acidity in zeolites with probe molecules? ACS Catal. 9 (2019) 1539–1548.
[15] R.A. van Santen, G.J. Kramer, Reactivity theory of zeolitic broensted acidic sites, Chem. Rev. 95 (3) (1995) 637–660.
[16] P. Cnudde, E.A. Redekop, W. Dai, N.G. Porcaro, M. Waroquier, S. Bordiga, M. Hunger, L. Li, U. Olsbye, V. Van Speybroeck, Experimental and theoretical evidence for the promotional effect of acid sites on the diffusion of alkenes through small-pore zeolites, Angew. Chem. Int. Ed. 60 (2021) 10016–10022.
[17] L.-E. Sandoval-Díaz, J.-A. González-Amaya, C.-A. Trujillo, General aspects of zeolite acidity characterization, Microporous Mesoporous Mater. 215 (2015) 229–243.
[18] A.A. Viggiano, R.A. Morris, F. Dale, J.F. Paulson, M.J. Henchman, T.M. Miller, A. E. Stevens Miller, Gas-phase acidities of metaphosphoric acid and metaphosphorus acid: enthalpies of deprotonation, Phys. Chem. 95 (1991) 1275–1277.
[19] J. Sauer, J.-R. Hill, The acidity of surface silanol groups. A theoretical estimate based on ab initio calculations on a model surface, Chem. Phys. Lett. 218 (1994) 333–337.
[20] R.A. van Santen, Theory of Brønsted acidity in zeolites, Stud. Surf. Sci. Catal. 85 (1994) 273–294.
[21] M. Brändle, J. Sauer, Acidity differences between inorganic solids induced by their framework structure. A combined Quantum mechanics/molecular mechanics ab initio study on zeolites, J. Am. Chem. Soc. 120 (1998) 1556–1570.
[22] E.A. Ivanova Shor, A.M. Shor, V.A. Nasluzov, G.N. Vayssilov, N. Rösch, Effects of the aluminum content of a zeolite framework: a DFT/MM hybrid approach based on cluster models embedded in an elastic polarizable environment, J. Chem. Theor. Comput. 1 (2005) 459–471.
[23] M. Rybicki, J. Sauer, Acidity of two-dimensional zeolites, Phys. Chem. Chem. Phys. 17 (2015) 27873–27882.
[24] A.J. Jones, R.T. Carr, S.I. Zones, E. Iglesia, The strength of brønsted acid sites in microporous aluminosilicates, J. Catal. 312 (2014) 58–68.
[25] A.J. Jones, E. Iglesia, The strength of brønsted acid sites in microporous aluminosilicates, ACS Catal. 5 (2015) 5741–5755.
[26] G. Noh, S.I. Zones, E. Iglesia, Consequences of acid strength and diffusional constraints for alkane isomerization and β-scission turnover rates and selectivities on bifunctional metal-acid catalysts, J. Phys. Chem. C 122 (44) (2018) 25475–25497.
[27] J.P. Perdew, K. Burke, M. Ernzerhof, Generalized gradient approximation made simple, Phys. Rev. Lett. 77 (1996) 3865.
[28] F. Neese, The ORCA program system, Wiley Interdiscip. Rev. Comput. Mol. Sci. 2 (2012) 73–78.
[29] F. Neese, Software update: the ORCA program system, version 4.0, Wiley Interdiscip. Rev. Comput. Mol. Sci. 8 (2017), e1327.
[30] F. Weigend, R. Ahlrichs, Phys. Chem. Chem. Phys. 7 (2005) 3297.
[31] F. Weigend, Phys. Chem. Chem. Phys. 8 (2006) 1057.
[32] E. Dib, I. Medeiros Costa, G.N. Vayssilov, H.A. Aleksandrov, S. Mintova, Complex H-bonded silanol network in zeolites revealed by IR and NMR spectroscopy combined with DFT calculations, J. Mater. Chem. 9 (2021) 27347–27352.
[33] R. Ditchfield, Mol. Phys. 27 (1974) 789.
[34] D. Massiot, F. Fayon, M. Capron, I. King, S. Le Calvé, B. Alonso, J.-O. Durand, B. Bujoli, Z. Gan, G. Hoatson, Magn. Reson. Chem. 40 (2002) 70–76.
[35] M. Bak, J.T. Rasmussen, N.C. Nielsen, SIMPSON: a general simulation program for solid-state NMR spectroscopy, J. Magn. Reson. 147 (2) (2000) 296–330.
[36] J. Yesinowski, H. Eckert, G.R. Rossman, Characterization of hydrous species in minerals by high-speed proton MAS-NMR, J. Am. Chem. Soc. 110 (1988) 1367–1375.
[37] G.N. Vayssilov, N. Rösch, Influence of alkali and alkaline earth cations on the brønsted acidity of zeolites, J. Phys. Chem. B 105 (2001) 4277–4284.
[38] G. Angelini, C.E. Johnson, J.I. Brauman, Addition and deprotonation in reactions of hydroxide ion with a β-hydroxysilane, Int. J. Mass Spectrom. Ion Process. 109 (1991) 1–14.
[39] R. Damrauer, R. Simon, M. Krempp, Effect of substituents on the gas-phase acidity of silanols, J. Am. Chem. Soc. 113 (1991) 4431–4435.